Journal of Molecular Structure 1200 (2020) 127016

Contents lists available at ScienceDirect

Journal of Molecular Structure

journal homepage: http://www.elsevier.com/locate/molstruc

Structural, spectroscopic and theoretical studies of sodium (2-carbamoylphenoxy) acetate salt

Alexandru Turza [a, b], Ana Maria Raluca Gherman [b, c], Vasile Chiș [b], Camelia Berghian-Grosan [a], Gheorghe Borodi [c, *]

[a] Department of Mass Spectrometry, Chromatography and Applied Physics, National Institute of R&D of Isotopic and Molecular Technologies, 67-103 Donat, 400293, Cluj-Napoca, Romania
[b] Faculty of Physics, Babes-Bolyai University, 1 Kogălniceanu, 400084, Cluj-Napoca, Romania
[c] Department of Molecular and Biomolecular Physics, National Institute of R&D of Isotopic and Molecular Technologies, 67-103 Donat, 400293, Cluj-Napoca, Romania

ARTICLE INFO

Article history:
Received 7 May 2019
Received in revised form
4 August 2019
Accepted 2 September 2019
Available online 4 September 2019

Keywords:
Algamon
Sodium (2-carbamoylphenoxy) acetate
Crystal structure
Density functional theory
Raman
FT-IR

ABSTRACT

Sodium (2-carbamoylphenoxy) acetate salt crystal belongs to the P-1 space group of triclinic system, Z = 2. The asymmetric part of the unit cell consists of four (2-carbamoylphenoxy) acetate (CBA) molecules. Three Na^+ ions are surrounded by six O atoms and one Na^+ ion is surrounded by five O atoms. The mean $Na1^+$ … O and $Na2^+$ … O distance is 2.47 Å while $Na3^+$ … O is 2.43 Å and $Na4^+$ … O is 2.49 Å. The supramolecular self-assembly of the four (2-carbamoylphenoxy) acetate molecules is realized by hydrogen bonds, and a variety of intermolecular interactions. The interactions within the bulk of the crystal structure were highlighted with Hirshfeld surfaces. FT-IR and Raman spectra of the studied compound are reported for the first time. Assignments of the normal modes was done with the aid of density functional theory frequency calculations on the monomer and two dimers, at B3LYP/6-311 + G(2d,p) level of theory.

1. Introduction

Sodium (2-carbamoylphenoxy) acetate salt, with the chemical formula $C_9H_8NNaO_4$ (Scheme 1), produced by Microsin (Bucharest, Romania) under the name of algamon [1], is the salt of the active substance *o*-carbamoyl-phenoxyacetic acid, used for its analgesic activity [2]. To our knowledge, the crystal structure of the product, further denoted as AGM, is not contained in the CSD 2018 database yet. The compound is appearing as solid white powder at room temperature, with a 263 °C melting point, and 419 °C boiling point.

The pharmacokinetics of sodium (2-carbamoylphenoxy) acetate was studied in 9 healthy male subjects following a single intramuscular administration and the plasma concentration of *o*-carbamoylphenoxyacetic acid and metabolised salicylamide was analysed. The plasma concentration profiles (AUC) were also monitored. It has been shown that there are moderate rates of metabolic conversion and only small amounts of salicylamide appear in the circulatory system [3].

The literature shows a lack of studies referring to this compound. In this paper, we report for the first time its structural characterization by X-ray single crystals diffraction, XRPD, and the characterization of intermolecular interactions with the surfaces Hirshfeld [4–8]. Vibrational properties of AGM are also reported herein. Its FT-IR and Raman spectra were registered for the first time. A full assignment of both spectra is listed. This was achieved with the aid of frequency calculations, by using density functional theory (DFT) methods. The calculated spectra, both IR and Raman, were performed on AGM monomer and two dimers, as being present in the crystal packing. Dimer models, able to capture intermolecular interactions, bring supplementary useful information related to vibrational features of molecules [9,10].

2. Experimental

Algamon was obtained from Microsin, a Romanian producer of active pharmaceutical ingredients, and was used without further

* Corresponding author. Department of Molecular and Biomolecular Physics, National Institute of R&D of Isotopic and Molecular Technologies, Donat 67-103, 400293, Cluj-Napoca, Romania.
E-mail address: borodi@itim-cj.ro (G. Borodi).

https://doi.org/10.1016/j.molstruc.2019.127016
0022-2860/

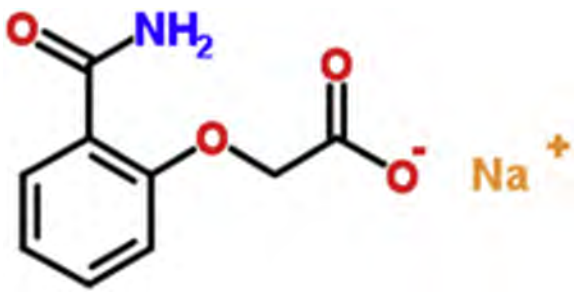

Scheme 1. Molecular scheme of sodium (2-carbamoylphenoxy) acetate.

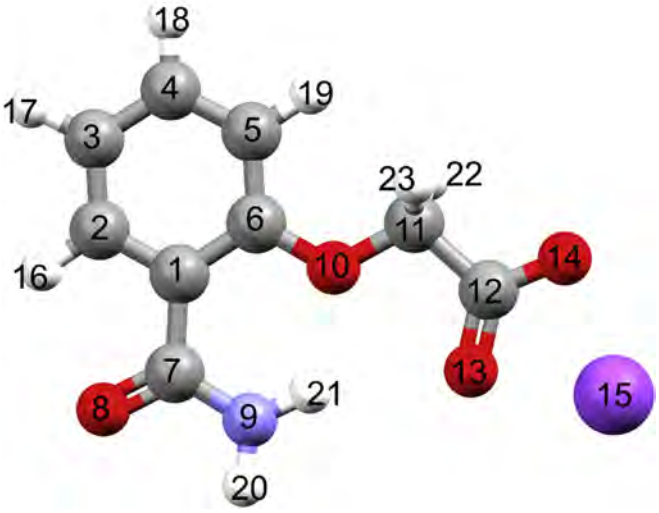

Fig. 1. Optimized geometry of AGM molecule at B3LYP/6-311 + G(2d,p) level of theory, in gas phase.

purification.

A suitable single crystal (0.3 × 0.2 × 0.1 mm) was selected from the bulk of crystalline powder; it was coated in inert oil (Paratone N), and mounted on a fine nylon loop. X-ray single crystal data collection was acquired by a SuperNova diffractometer equipped with dual microsources, Eos CCD detector with the tube operating at 50 kV and a current of 0.8 mA using Cu Kα radiation, the crystal being kept at room temperature during data acquisition.

Powder X-ray diffraction pattern was recorded on a Bruker D8 Advance diffractometer, equipped with a germanium (1 1 1) monochromator in the incident beam to get a monochromatic radiation (Cu $K\alpha_1$). Data acquisition was made with DIFFRAC plus XRD Commander software, having a scan speed of 0.02° s^{-1} in 3-40° 2θ range.

Crystallographic data for the structure reported in this paper have been deposited with the Cambridge Structural Database as Supplementary Publication CCDC No 1909666.

Raman spectrum was collected with a Raman JASCO NRS 3300 spectrometer, equipped with a CCD detector (−69 °C), a diffraction grating of 600/mm, and a 100× Olympus objective. 785 nm laser line was used as an excitation source, its power being set at 137.6 mW. The resulted Raman spectrum is an addition of three acquisitions of 120 s each. It was recorded with a resolution of 6.45 cm^{-1}.

FT-IR spectrum of AGM was collected with a JASCO 6100 spectrometer, with a resolution of 2 cm^{-1}, using KBr pellet technique. The spectrum was recorded in the range of 350−4000 cm^{-1}.

Influence of acidic media onto the sodium (2-carbamoylphenoxy) acetate: the salt was treated with 0.2 M hydrochloric acid, considering a 1: 1.1 M ratio between salt and HCl. Thus, to 100 mg of salt, 2.53 mL solution of 0.2 M hydrochloric acid is added. In a very short time a white precipitate was obtained. It was analysed by X-ray diffraction and the presence of NaCl was detected in the obtained mixture. Further, the precipitate was washed with double distilled water to remove the sodium chloride.

2.1. Computational details

Single crystal diffraction data were collected using CrysAlis PRO software and crystal structure was solved with Olex2 [11], by olex2.solve [12] structure solution program using Charge Flipping and refined with the ShelXL [13] refinement package by least Squares minimization. Absorption correction was made by multi-scan method in CrysAlis PRO software using spherical harmonics, implemented in SCALE3 ABSPACK scaling algorithm [14].

Hydrogen atoms attached to C, N and O atoms were positioned geometrically and refined as riding atoms, considering $U_{iso}(H) = 1.2U_{eq}(C,N)$ for all CH, CH_2 and NH_2 groups and $1.5U_{eq}(O)$ for all OH_2 groups. Water molecule was refined as rotating group

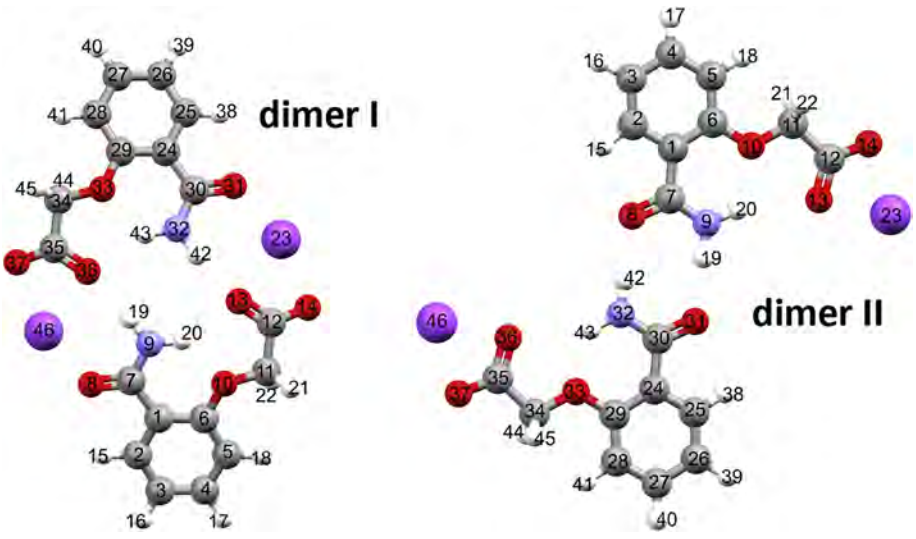

Fig. 2. Optimized geometry of AGM dimer I, and II at B3LYP/6-311 + G(2d,p) level of theory, in gas phase. Labels from the monomer are kept the same for both dimers.

Table 1
Crystal data and structure refinement for sodium (2-carbamoylphenoxy) acetate.

Identification code	sodium (2-carbamoylphenoxy) acetate
Empirical formula	$C_{36}H_{34}N_4Na_4O_{17}$
Formula weight	886.63
Temperature/K	293(2)
Crystal system	triclinic
Space group	P-1
a/Å	10.8538(4)
b/Å	13.6231(6)
c/Å	13.8545(6)
α/°	103.770(4)
β/°	103.723(3)
γ/°	100.065(3)
Volume/Å^3	1873.95(13)
Z	2
ρ_{calc}g/cm^3	1.571
μ/mm^{-1}	1.460
F(000)	916.0
Crystal size/mm^3	0.3 × 0.2 × 0.1
Radiation	CuKα (λ = 1.54184)
2Θ range for data collection/°	6.89 to 142.896
Index ranges	−13 ≤ h ≤ 10, −16 ≤ k ≤ 16, −17 ≤ l ≤ 14
Reflections collected	11851
Independent reflections	7113 [R_{int} = 0.0170, R_{sigma} = 0.0224]
Data/restraints/parameters	7113/0/551
Goodness-of-fit on F^2	1.038
Final R indexes [I > =2σ (I)]	R_1 = 0.0343, wR_2 = 0.0974
Final R indexes [all data]	R_1 = 0.0380, wR_2 = 0.1009
Largest diff. peak/hole/e Å^{-3}	0.29/-0.24

with O–H = 0.878 Å. Secondary CH_2 were refined with riding coordinates, with C–H = 0.97 Å, aromatic H atoms were refined as riding with C–H = 0.93 Å, while primary amide with riding coordinates and N–H = 0.86 Å.

Hirshfeld analysis was used to provide data about interactions within the bulk of a crystal structure, which are mapped on a 3D surface [15,16]. Based on the CIF file obtained by single crystal X-ray diffraction, Crystal Explorer software [17] was used to calculate the Hirshfeld surface and color mapping. During the computation, the X–H bond lenghts (where X = C, O, or N) were normalized at standard bond lenghts determined by neutron diffraction (C–H = 1.083 Å, O–H = 0.983 Å and N–H = 1.009 Å). Fingerprints [18,19] are 2D representations designed to visualize different interactions in a quantitative manner, as percentages. Every individual molecule has an unique Hirshfeld surface and fingerprint plot which are influenced by its environment. Fingerprint plot was done using d_{norm} function, where d_{norm} (Eq. (1)) is a ratio encompassing the distances of any surface point to the nearest interior (d_i) and exterior (d_e) nucleus, and the van der Waals radii of the atoms. For each point on the Hirshfeld surface, d_e and d_i are both determined, each point on the 2D fingerprint plot corresponding to a unique pair (d_e and d_i). Red spots on the Hirshfeld surface denote that d_{norm} has a negative value, thus the sum of d_i and d_e is less than the sum of the van der Waals radii. White spots indicate that the sum of d_i and d_e is equal to zero, and intermolecular connections are close to the sum of van der Waals radii. Finally, blue indicates a positive value for d_{norm} function, where the intermolecular contacts are longer compared to the sum of van der Waals radii.

$$d_{norm}=\frac{d_i - r_i^{vdW}}{r_i^{vdW}}+\frac{d_e - r_e^{vdW}}{r_e^{vdW}} \quad (1)$$

Density Functional Theory (DFT) methods, implemented in Gaussian 09, Revision E.01 software package [20], were employed on both geometry optimizations and frequency calculations. The level of theory used is a joining of B3LYP [21–24] hybrid exchange-correlation functional and 6-311 + G(2d,p) triple-zeta basis set. Wavefunction convergence and geometry optimization were met using tight criteria and an ultrafine grid. Both geometry optimization and frequency calculations were performed on algamon monomer (Fig. 1) and two of its dimers (Fig. 2). There are two ways in which two algamon molecules can form hydrogen bonds in the crystallographic network, thus the two dimers. All starting geometries were taken from the crystallographic data. Frequency calculations confirmed that the geometries correspond to true minima on the potential energy surface. Calculated bond lenghts, angles and dihedrals of AGM monomer, dimer I, and dimer II are listed in Tables S3, S4, and S5. The calculated wavenumbers were scaled by the corresponding scaling factor of the used level of theory (0.967) as suggested by Andersson and Uvdal [25]. Normal modes assignment to their specific IR and Raman bands was made by observation of animated modes by using GaussView, Version 5 [26] software. We took into account both the relative intensities and peaks' position of the resulted calculated Raman and IR spectra. All calculations were performed in gaseous phase.

Molecular structures of AGM monomer and the dimers were pictured in Mercury [27], as well as crystal packing, hydrogen bonds and short range interactions.

All Raman and IR spectra, both calculated and experimental, were ploted in Origin (OriginLab, Northampton, MA).

3. Results and discussions

3.1. Crystal structure

3.1.1. Single crystal data and molecular configuration

Crystals of sodium (2-carbamoylphenoxy) acetate ($C_9H_8NNaO_4$; M = 217.154 g/mol) are triclinic, belong to the space group P-1 and have the following unit cell parameters: a = 10.8538(4) = Å, b = 13.6231(6) Å, c = 13.8545(6) Å, α = 103.770(4)°, β = 103.723(3)°, γ = 100.065(3)°. No restraints and constraints

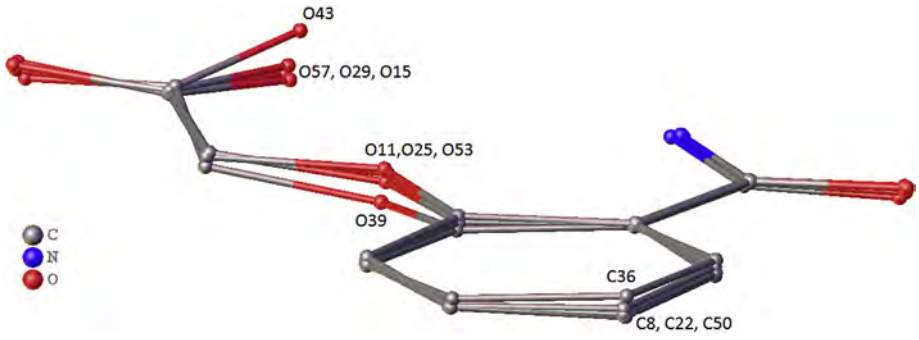

Fig. 3. Overlay of the four sodium (2-carbamoylphenoxy) acetate molecules forming the asymmetric unit.

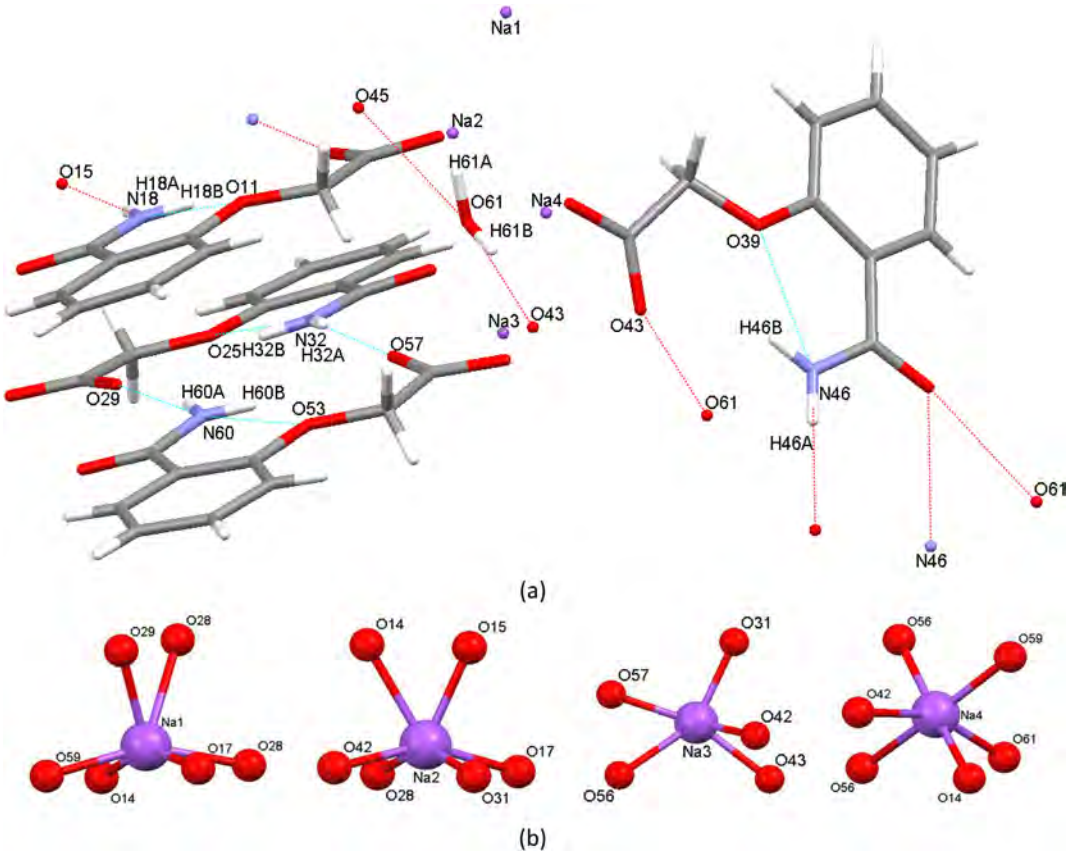

Fig. 4. (a) Inter (red dotted lines) and intramolecular (blue dotted lines) hydrogen bonds within the asymmetric unit of sodium (2-carbamoylphenoxy) acetate; (b) coordination of the four Na ions.

were used during refinement procedure. All information about crystal structure and refinement are displayed in Table 1.

The four molecules in the asymmetric unit were overlapped (Fig. 3) using Olex2 software in order to highlight the differences between their configurations. It can be observed that these differences are not very large. The most notable are present in the acetate group and the oxygen atoms (O11, O25, O39, and O53) between the acetate group and the carbamoylphenoxy benzene ring. Small configuration differences, but still noticeable, can be observed are in the amide group. Finally, in the unit cell, three of the four AGM molecules exhibit similar configuration, one of them being slightly different, as it can be seen in Fig. 3. The O43, O39 oxygen atoms and C36 carbon belong to the same molecule, and all of them have different position, compared with the corresponding O atoms from the other three molecules.

3.2. Na cations coordination

In the crystal structure, the asymmetric unit for sodium (2-carbamoylphenoxy) acetate is composed of four such molecules, being coordinated to four Na atoms. The sodium cations are coordinated to oxygen atoms, coordination being five or six, as seen in Fig. 4b, together with their geometries. All O—Na distances and O—Na—O angles are listed in Tables S1 and S2, respectively. The Na—O coordination distances values are within a fairly narrow range 2.317—2.738 Å, the maximum difference being slightly over 0.4 Å. Three of the four Na atoms are coordinated by oxygen atoms belonging to the acetate fragment, while the last is linked by the oxygen from amide group. Mean Na—O bond lengths are comparable to those in similar compounds [28,29].

Table 2
Intermolecular (* - red doted lines in Fig. 4a) and intramolecular (^ - blue dotted lines in Fig. 4a) hydrogen bond lengths, within the asymmetric unit of sodium (2-carbamoylphenoxy) acetate.

D-H … A	d(D-H)	d(H … A)	d(D … A)	<(DHA)
*(amide)N46—H46A … O45	0.860	2.0982(17)	2.9455(17)	168.30(5)
*(water)O61—H61A … O45	0.860	2.306(6)	3.0271(16)	139.4(8)
*(amide)N18—H18A … O15	0.878	2.0878(15)	2.9208(15)	162.92(5)
*(water)O61—H61B···O43	0.878	1.895(4)	2.7606(16)	168.3(16)
^N60—H60B···O53	0.860	1.9637(16)	2.6282(16)	133.19(5)
^N60—H60B···O57	0.860	2.5239(16)	3.3404(16)	158.85(4)
^N60—H60A … O29	0.860	2.102(16)	2.9295(16)	161.25(5)
^N18—H18B···O11	0.860	1.9433(15)	2.6105(15)	133.44(5)
^N18—H18B···O15	0.860	2.5518(16)	3.3659(16)	158.29(3)
^N32—H32B···O25	0.860	1.9362(16)	2.6077(16)	133.96(5)
^N32—H32A … O57	0.860	2.1529(17)	2.9654(17)	157.42(5)
^N46—H46B···O39	0.860	1.9296(17)	2.5981(17)	133.57(5)
^N46—H46B···O43	0.860	2.4085(17)	3.2060(17)	154.47(4)

Table 3
Distances (in Å) for the different types of short range interactions in the crystal packing.

Interaction	Distances (Å)	No/asymm unit
Na—Na	3.485—3.991	4
Na-π	3.140—3.821	4
Na—C	2.871—3.498	8
C—H···Na	3.079—3.393	4
N—H···Na	3.046—3.240	3

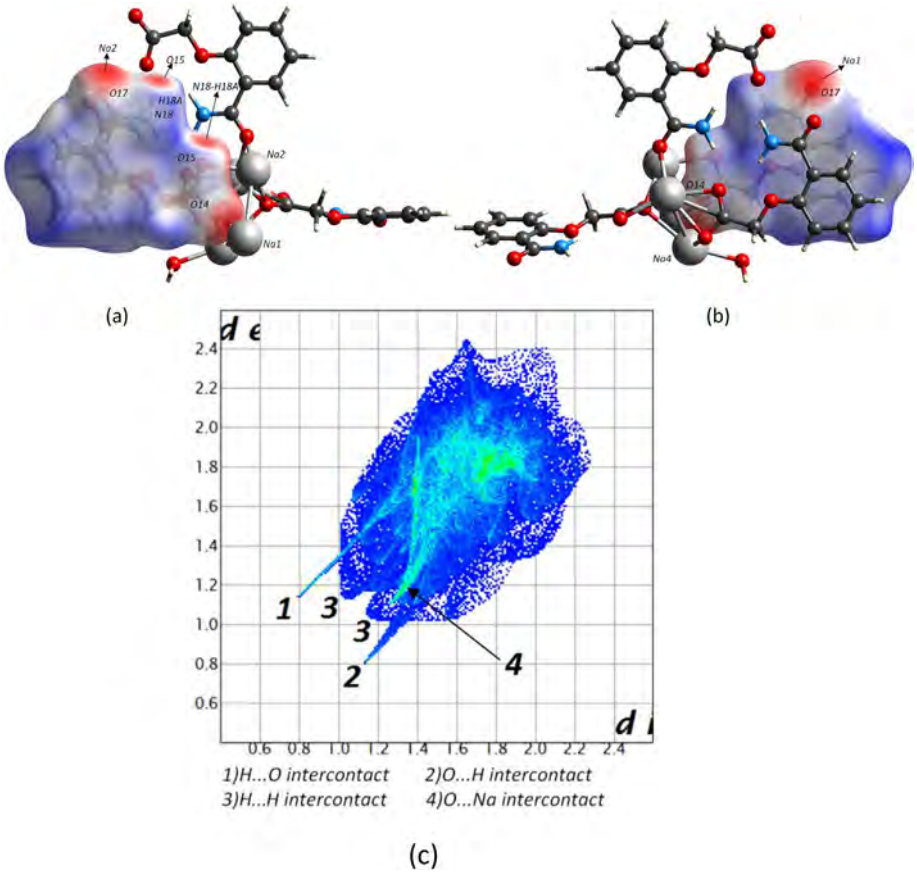

Fig. 5. Front view (a), back view (b) of the Hirshfeld surface mapped with d_{norm} over the range −0.6842 to +1.1678 arbitrary units and fingerprint plot (c) for the CBA molecule including N18 atom.

Na cations are positioned on both sides of the crystallographic plane (0 0 1), in proximity of this plane, as seen in Fig. S1. The atoms with the same label are connected one by one through inversion operation.

3.3. Hydrogen bonds and short range interactions

Among the three (2-carbamoylphenoxy) acetate molecules from the asymmetric unit, for which the acetate fragments coordinates the sodium cations, one of them forms the N46—H···O45 intermolecular hydrogen bond with the amide group. The second molecule forms a hydrogen bond with the amide group N18—H···O15, while the last one does not interact at all with its neighbours by intermolecular hydrogen bonds. This is the AGM monomer for which the oxygen from amide coordinates one Na atom. Two intermolecular hydrogen bonds starting from the water molecule (O61), where O61 is the donor, form the O61—H61B ··· O43 and O61—H61A … O45 intermolecular bonds. There are also nine intramolecular hydrogen bonds bridging the nitrogen atoms of the amides with the acetate and amide oxygens of (2-carbamoylphenoxy) anions, which are presented in the second part of Table 2. All the above mentioned hydrogen bonds can be seen in Fig. 4a.

By omitting the sodium cations within the structure it is observed that the crystal structure may be reduced to three synthons held by N—H···O and O—H···O hydrogen bonds between the (2-carbamoylphenoxy) acetate anions.

Two (2-carbamoylphenoxy) acetate anions are coupled by double N46—H46A … O45 hydrogen bond, characterized by a $R_2^2(8)$ intermolecular descriptor. Also the two (2-carbamoylphenoxy) acetate (CBA) molecules are linked by bridged water molecules through the O61—H61B ··· O43 bond with acetate group and O61—H61A … O45 hydrogen bond from the amide group. The (2-carbamoylphenoxy) acetate anions and water molecules are related by an inversion operation, having the centroid coordinates at (0, ½, ½) and which is a special position and an inversion point of the P-1 space group (Figure S2 A).

A different supramolecular synthon, forming a $R_2^2(18)$ motif is built via double N18—H18A … O15 intermolecular hydrogen bonds. The synthon is generated by the inversion of a (2-carbamoylphenoxy) acetate anion, having the centroid positioned on the center of ***oa*** edge (½, 0, 0), which is an inversion point of the P-1 space group and a special position (Figure S2 B).

Another supramolecular synthon is generated by coupling two (2-carbamoylphenoxy) acetate anions from asymmetric unit via N32—H32A … O57, respectively N60—H60A … O29 hydrogen bonds. The assembly is characterized by a $R_2^2(18)$ descriptor having the anions related by pseudo-inversion with the centroid localized in general positions (0.576, 0.76, 0.063) (Figure S2 C).

Besides the hydrogen bonds, the crystal structure stability is also held by short range interactions, as given in Table 3.

3.4. Hirshfeld analysis

The analysis was conducted individually for each fragment of (2-carbamoylphenoxy) acetate in the asymmetric unit and the water molecule as well. Hirshfeld surfaces were generated presenting front and back views, with the Na ions being always outside of the

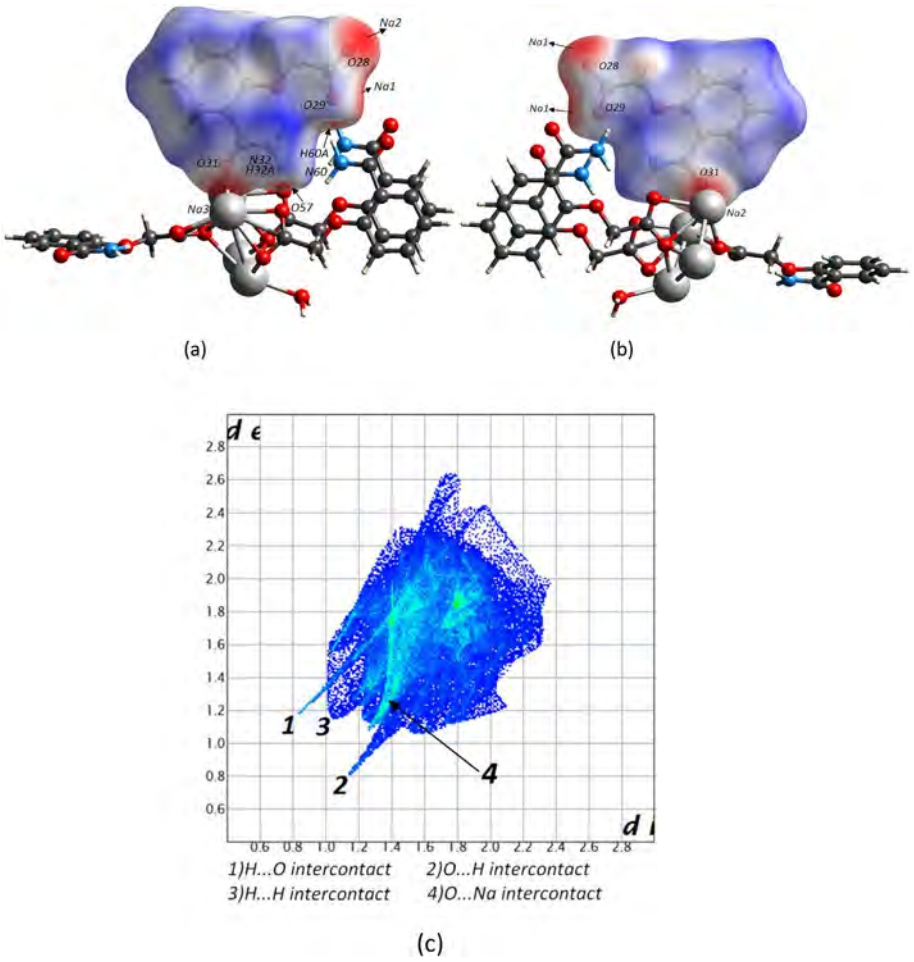

Fig. 6. Front view (a), back view (b) of the Hirshfeld surface mapped with d_{norm} over the range −0.6903 to +1.1672 arbitrary units and fingerprint plot (c) for the CBA molecule including N32 atom.

surfaces.

The Hirshfeld surface mapped with d_{norm} for (2-carbamoylphenoxy) acetate fragment (Fig. 5a and b) which include the N18 atom shows two red spots which are included in the formation of $R_2^2(18)$ supramolecular synthon via the N18—H18A … O15 hydrogen bond (Figure S2 B). These two hydrogen bonds are identified on the fingerprint plot by H···O and O···H interactions as two sharp spikes labeled by 1 and 2 (Fig. 5c). Five deep red spots are present on the Hirshfeld surface and are associated with the coordinative interaction with Na1, Na2 and Na4 cations (Fig. 5a and b). This feature is signaled on the fingerprint plot by an intense green area labeled by 4.

The (2-carbamoylphenoxy) acetate fragment which include N32 atom exhibits two red spots mapped on the Hirshfeld surface (Fig. 6a and b), indicating the formation of two intermolecular hydrogen bonds, namely N32—H32A … O57 (N32—H32 being inside the Hirshfeld surface) respectively N60—H60A … O29 (O29 being inside the Hirshfeld surface), which participate to the formation of the $R_2^2(18)$ synthon (Figure S2 C). Six deep red spots are present on the surface and are characteristic to Na—O (Na1, Na2, and Na3) coordinative interactions (seen on the fingerprint plot in Fig. 6c as label 4).

The amide group of the (2-carbamoylphenoxy) acetate fragment, including the N46 atom, builds a $R_2^2(8)$ graph set motif via the two N46—H46A … O45 hydrogen bonds (Figure S2 A), which are seen as two adjacent red spots on the Hirshfeld surface (Fig. 7a and b). Additionally, two hydrogen bonds O61—H61B···N43 and O61—H61A … O45 are identified on the surface as red areas, O61 being the oxygen from water. Four coordinative interactions with the Na2, Na3 and Na4 cations are also seen on the surface.

The Hirshfeld surface mapped on the fragment containing the N60 atom shows two red spots as an indication of N32—H32A … O57 respectively N60—H60B···O29 hydrogen bonds formation (Fig. 8a and b) which builds a $R_2^2(18)$ graph set motif (Figure S 2C) between the two (2-carbamoylphenoxy) acetate anions. The coordination with five Na cations (Na1, Na3 and Na4) is represented as deep red spots on the surface.

For water molecule, the Hirshfeld surface mapped with d_{norm} shows the coordinative contact as an intense red spot in the proximity of Na4 cation (Fig. 9a and b). The O61—H61B···O43 and O61—H61A … O45 hydrogen bonds are illustrated as two red spots, O61 being the oxygen from water. The 2D representation of the Hirshfeld surface (the fingerprint plot) shows a sharp spike characteristic to O—H···O hydrogen bonding (label 1, Fig. 9c). The O61—Na4 coordination is represented on the Hirshfeld surface as a red spot and transposed on the fingerprint plot as label 4.

It can be noted that the fingerprint plots for the four molecules are quite similar; spike 1 and 2 represents the H···O and O···H contacts, label 3 indicates the H···H contacts while the O···Na contacts are shown by label 4.

Therefore, Hirshfeld analysis for all four CBA molecules and water revealed that the strongest interactions are hydrogen bonds

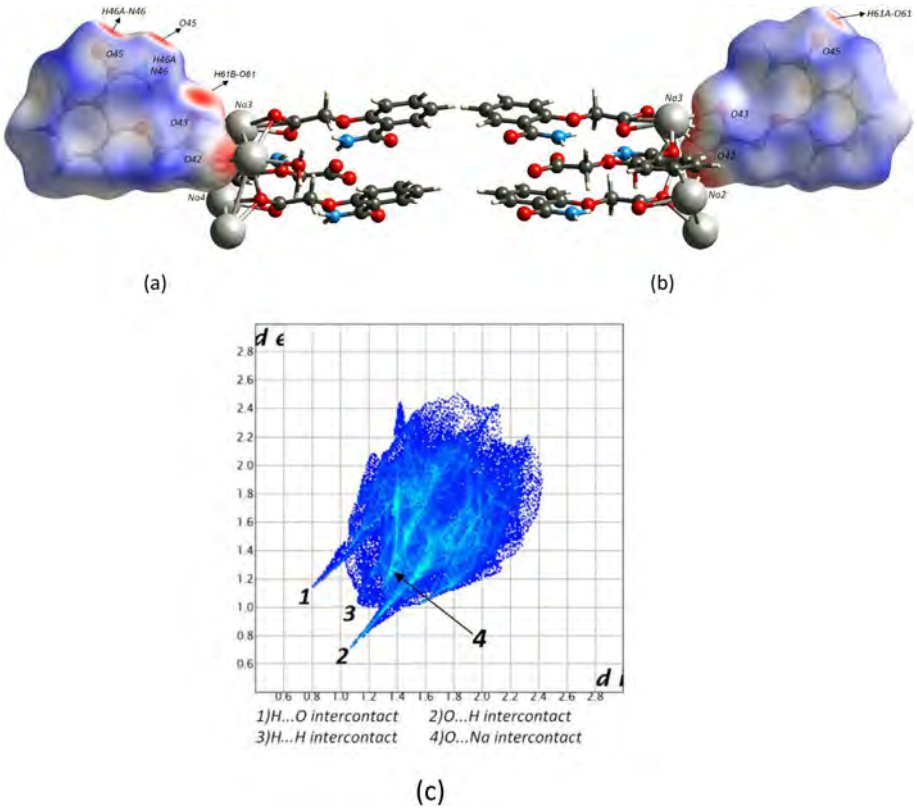

Fig. 7. Front view (a), back view (b) of the Hirshfeld surface mapped with d_{norm} over the range −0.6595 to +1.2012 arbitrary units and fingerprint plot (c) for the CBA molecule including N46 atom.

that contribute to the formation of supramolecular synthons and the interactions between oxygen atoms and Na cations. However, the percentage contributions of interatomic contacts to the Hirshfeld surface shows that the highest number of interactions correspond to H···H contacts, followed by O···H/H···O, C···H/H···C and O···Na contacts, as shown in Fig. 10. Yet, for the water molecule, the number of H···H and O···H/H···O interactions is almost equal.

4. Vibrational spectroscopy. IR and Raman spectra

Vibrational (especially Raman) spectroscopy is an important tool for the pharmaceutical field, both in the development and manufacturing stages, proving significant information in the process of drug production [30]. Thus, a full description of both Raman and IR bands are very important for any pharmaceutical drug. The AGM Raman and IR bands are presented in Table 4, along with a full assignment of the normal modes. The observed bands (Figs. 11 and 12) are classified by their intensities as very weak, weak, medium, strong, and very strong.

In the high wavenumber region (above 1800 cm^{-1}) the vibrational spectrum has been recorded by using FT-IR spectroscopy, Fig. 11. We assigned symmetric and asymmetric stretching of NH_2 group to the medium 3414 cm^{-1} and small 3590 cm^{-1} IR bands. They are very well approximated by frequency calculations on AGM monomer, at 3417 and 3565 cm^{-1}.The very small IR bands above 2900 cm^{-1} represent different stretches of CH and CH_2 units. Most of the corresponding calculated wavenumbers are in better agreement for dimer II. This fitting is in accordance with the one between the calculated and XRD geometrical parameters (bond lengths, angles and dihedrals) for dimer II, as seen in Table S3 − S5.

There are several bands in the 1500–1700 cm^{-1} range, which correspond mainly to NH_2 bending moiety, one of them being the 1560 cm^{-1} frequency; it is of medium intensity in the Raman spectrum, Fig. 12, and a weak shoulder, in the IR spectrum, slightly shifted to 1567 cm^{-1}. In Table 4 we report a set of two wavenumbers for each mode, corresponding to both NH_2 groups, one for each molecule in a dimer. NH_2 chemical group is involved in both inter and intramolecular hydrogen bonds, what brings the differences in corresponding calculated bonds of the monomer and two dimers. The other one is one of the strongest Raman band, at 1591 cm^{-1}, and has an IR correspondent shifted to 1600 cm^{-1}. The calculated bands of both dimers perfectly match the experimental values (1591 and 1594 cm^{-1} for dimer I; 1590 and 1596 cm^{-1} for dimer II). In the IR spectrum, for the moieties grouped in a broad band with several peaks, all calculated correspondents are underestimated with a significant amount. 1625 cm^{-1} is one of the strongest intensities in the whole spectrum, and does not have a Raman correspondent. Best calculated results were obtained in the case of the two dimers.

The bands between 1250 and 1500 cm^{-1}, of complementary IR/Raman medium or weak intensity, are mainly due to either CC stretching, or CH_2 wagging.

The weak band at 1446 cm^{-1} (Raman) or 1442 cm^{-1} (IR) is due to the bending vibration of NH_2 unit.

CH_2 twisting is assigned to the weak Raman 1222 cm^{-1}, or IR 1224 cm^{-1} peak. It is best reproduced by the two dimers, with a difference of 17 and 19 cm^{-1}.

The two strong Raman bands at 1153 cm^{-1} and 1167 cm^{-1}, and their IR correspondents, at 1152 and 1163 cm^{-1}, are due to an in plane bending of CH groups.

NH_2 rocking is assigned to the strong Raman band at 1117 cm^{-1}, with very weak IR intensity.

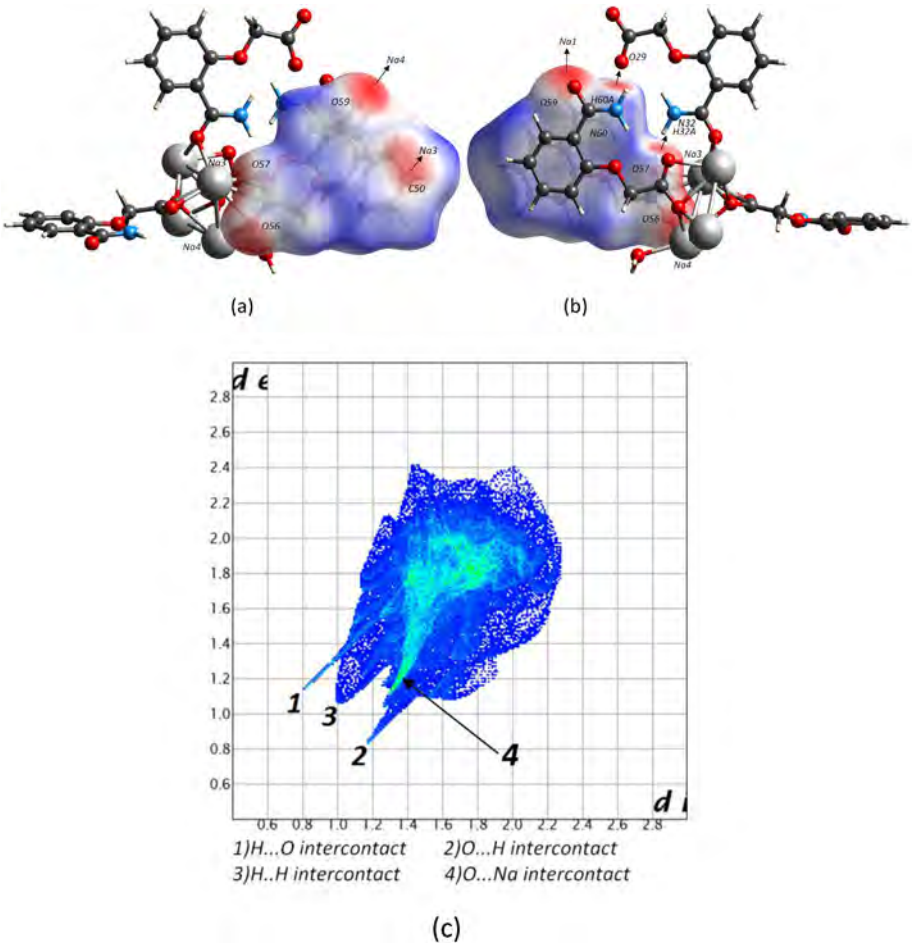

Fig. 8. Front view (a), back view (b) of the Hirshfeld surface mapped with d_{norm} over the range −0.7055 to +1.2092 arbitrary units and fingerprint plot (c) for the CBA molecule including N60 atom.

CN stretching is assigned to the medium Raman and weak IR band, observed at 1095 cm^{-1}, and 1097 cm^{-1}, respectively. The calculated values are best reproduced for the two dimers, with shifts from experimental counterparts between 2 and 10 cm^{-1}. We obtained a set of two values for each dimer. CO stretching is assigned to the weak Raman shoulder at 1054 cm^{-1}, and weak IR band at 1053 cm^{-1}. Moreover, this band represents an in plane deformation of benzene ring.

Benzene ring breathing can be observed as a strong Raman band at 1042 cm^{-1}, and a weak IR, at 1044 cm^{-1}. The results for all three systems present close values, 1030 cm^{-1} being the best.

C11C12 stretching, coupled with O═C─O bending, can be observed as a strong Raman band at 935 cm^{-1}, and a very weak IR band, at 934 cm^{-1}. This band is best reproduced in the case of dimer I (937 cm^{-1}), as expected, since the mentioned atoms are involved in hydrogen bonds between two AGM molecules, bonds that are always present in AGM crystal, as seen in Fig. 4a.

The weak band at 850 cm^{-1}, existing in both Raman and IR spectrum, is attributed to an in plane deformation of the benzene ring, more specifically, it consists of a CCC bending and an in plane bending of CH groups. This band's shape is very well reproduced in the calculated Raman spectrum of both dimers, together with the very weak shoulder.

NH_2 twisting is assigned to the very strong Raman band at 763 cm^{-1}, and the very weak shoulder, at 796 cm^{-1}. In the IR spectrum, this band is of weak intensity. Again, the correspondent calculated on dimer I is in the best agreement (762 cm^{-1}) with the experimental data, the NH_2 groups in this configuration being involved in inter and intramolecular hydrogen bonds.

In phase out of plane bending of CH group is assigned to the medium band at 750 cm^{-1}. This band is present only in the IR spectrum.

O═C─O bending can be observed in the Raman spectrum with medium intensity (701 cm^{-1}) and with weak intensity in the IR spectrum (699 cm^{-1}). The calculated wavenumber corresponding to dimer I is in the best agreement with experimental data, hydrogen bonds which involve the above mentioned atoms being satisfied in this configuration.

The weak Raman and medium IR band observed at 623 cm^{-1} is due to an in plane deformation of the benzene ring, a combination of NH_2 rocking and CCC bending. Its very weak Raman shoulder or the medium IR band, observed at 612 cm^{-1}, and 617 cm^{-1} respectively, are assigned to CH_2 rocking and O═C─O wagging.

The band at 474 cm^{-1} presents medium intensity in the Raman spectrum and weak intensity in the IR spectrum. In the latter case, it can be observed slightly shifted, at 480 cm^{-1}. This band is assigned to NH_2 rocking. The corresponding value calculated on the AGM monomer is in a closer proximity with the Raman value, while those calculated on dimers are in better agreement with the value in the IR spectrum.

Raman band observed at 412 cm^{-1} is the strongest and is attributed to an in plane deformation of AGM molecule. In the IR

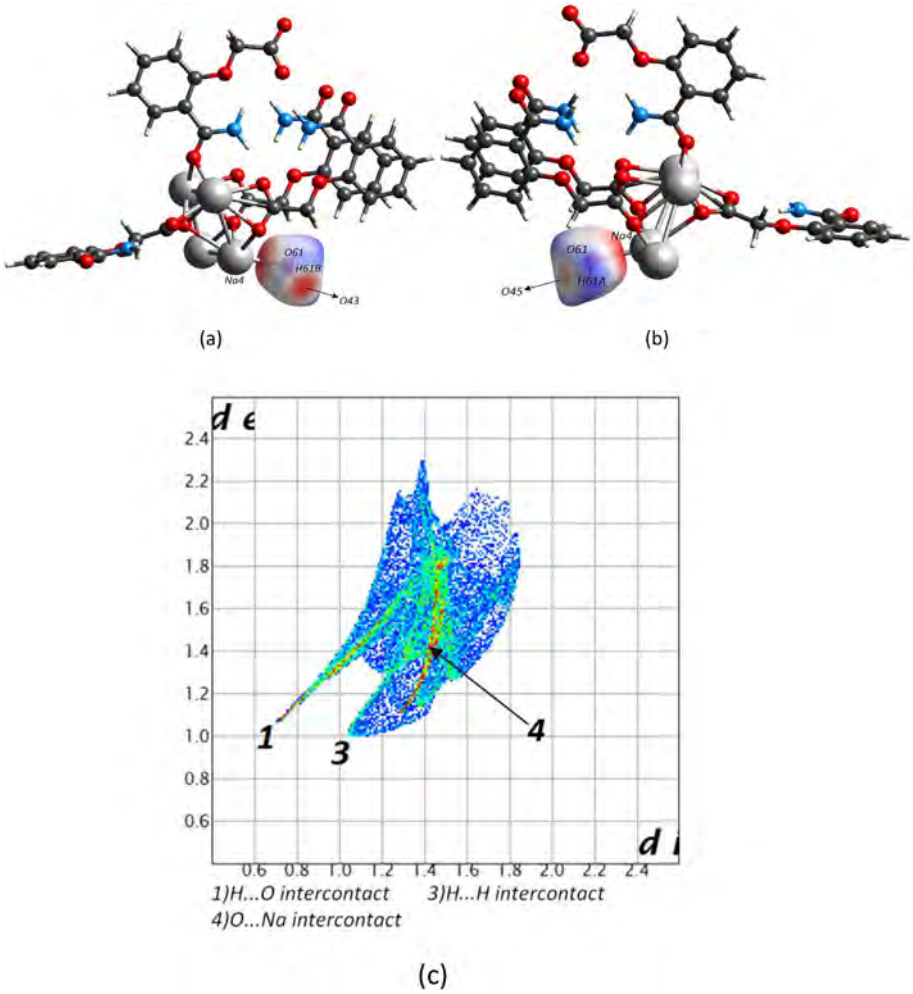

Fig. 9. Front view (a), back view (b) of the Hirshfeld surface mapped with d_{norm} over the range −0.6566 to +1.0870 arbitrary units and fingerprint plot (c) for the water molecule.

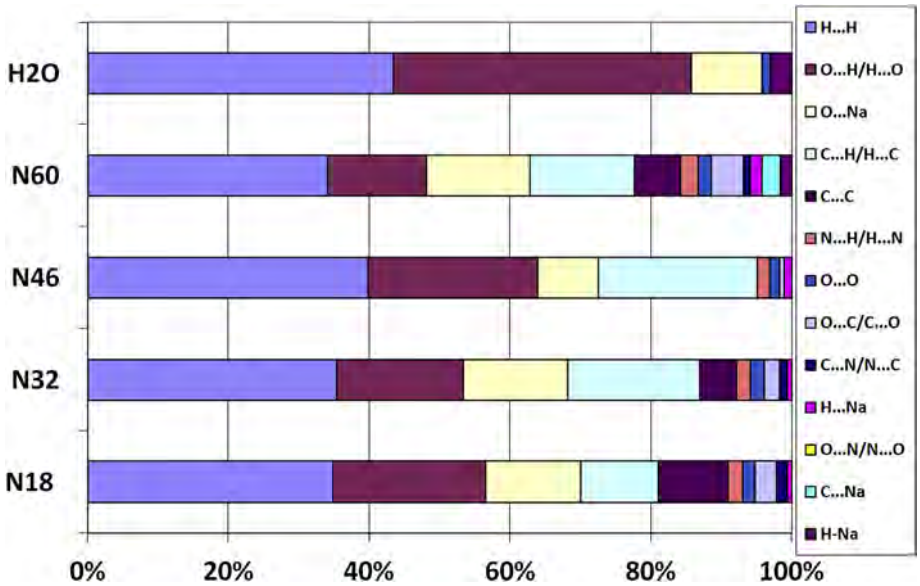

Fig. 10. Percentage contributions to the Hirshfeld surface area for the various close intermolecular contacts for the different CBA fragments and water molecule. N60, N46, N31, N18 represents the molecules which include these atoms.

Table 4
Experimental Raman and FT-IR bands of AGM molecule, together with full assignments based on DFT calculations, performed on the monomer and the two considered dimers of the molecule of interest. All calculations were done in gas-phase, at B3LYP/6-311 + G(2d,p) level of theory.

Experimental		Calculated			Assignments
Raman	IR	monomer	dimer I	dimer II	
154 m	–	152	145	156	ρ(CH_2), τ(benzene ring)
	–	–	160	–	ρ(CH_2), τ(benzene ring) in phase monomers
	–	181	173; 181	183; 188	ρ(benzene ring), β(side chains) (ν_{HB}(O10H20))
	–	214	234; 244	214; 216	ρ(benzene ring), β(side chains) (ν_{HB}(O13H20))
269 vs	–	252	270	258	τ(benzene ring)
	–	286	284	294	ρ(benzene ring), ρ(formamide), ν(O14Na15), ρ(O13C12O14)
358 m	354 w	338	306	349; 350	ρ(AGM) − ρ(NH_2), ρ(benzene ring), ρ(O13C12O14)
_	364 w	359	371; 380	364; 376	ρ(AGM) − ω(CH_2), β(C1C7N9), ρ(NH_2)
412 vs	408 vw	401	427	402; 421	in plan def. of AGM − ν(C1C7), ρ(NH_2), β(O8C7N9), δ(CH), ω(CH_2)
		412	–	–	ω(NH_2)
_	428 vw	448	446	–	ω(NH_2), τ(CH) out of phase
474 m	480 w	477	481; 485	481; 488	ρ(NH_2), ρ(O13C12O14), ω(CH_2), δ(CH)
526 vw	529 vw	539	543	542; 543	τ(CH) out of phase, τ(NH_2)
580 w	567 w	580	582	581; 585	β(C6O10C11), δ(CH), ρ(NH_2), ω(CH_2)
591 s h w	–	606	599	609; 610	β(C1C6C5), β(C2C3C4) − in plane deformation of benzene ring, ν(C11C12), ρ(NH_2), β(O13C12O14), β(O8C7N9)
612 s h vw	617 m	623	617	622	ρ(CH_2), ω(C12O13O14)
623 w	623 s h m	625	642	645	ρ(NH_2), β(C1C2C3), β(C4C5C6) − in plane deformation of benzene ring
		–	655	640	ω(NH_2)
681 s h vw	675 w	656	694	–	τ(NH_2), τ(CH) out of phase
701 m	699 w	714	708	719; 722	β(O13C12O14), ρ(NH_2), β(C2C1C6), β(C3C4C5) − in plane deformation of benzene ring
		–	721	–	ω(NH_2)
_	750 m	767	773	766	τ(CH) in phase
763 s	765 s h w	764	762; 786	774; 778	τ(NH_2), ν(C1C7), β(C2C1C6), β(C3C4C5), δ(CH) − in plane deformation of benzene ring, β(O13C12O14), β(C6O10C11)
796 vw	798 vw	805	819	799; 800	τ(NH_2), τ(CH) out of phase, ω(C1C7O8)
850 w	850 s h w	862	861	864	β(C2C3C4), δ(CH) − in plane deformation of benzene ring, β(C5C6O10), ρ(NH_2)
		868	877	874	τ(CH) out of phase − out of lane deformation of benzene ring
935 s	934 vw	945	937	945	ν(C11C12), β(O13C12O14), ω(CH_2)
1042 s	1044 w	1029	1030	1030	benzene ring breathing, δ(CH)
1054 s h w	1053 w	1042	1016	1041	ν(O10C11), β(C3C4C5), δ(CH) − in plane deformation of benzene ring
1095 m	1097 w	1083	1093; 1103	1101; 1105	ν(C7N9), ρ(NH_2), δ(CH), ν(C11O10)
1117 s	1117 vw	1060	1075; 1079	1075; 1076	ρ(NH_2), β(C1C6C5), δ(CH)
1153 s	1152 w	1125	1130	1130; 1132	δ(CH), ρ(NH_2)
1167 s	1163 w	1147	1147	1146	δ(CH)
1222 w	1224 w	1208	1205	1205	τ(CH_2)
1252 m	1252 m	1227	1227; 1230	1229; 1230	ν(C6O10), ν(C1C2), ν(C4C5), δ(CH), ω(CH_2)
		1252	1256; 1257	1256; 1257	β(C5C1C7), δ(CH), ρ(NH_2), ω(CH_2)
1278 w	1279 m	1280	1279	1279; 1280	ν(C1C2), ν(C3C4), ν(C5C6), δ(CH) − in plane deformation of benzene ring, β(NH_2)
1301 w	1301 s h w	1312	1311	1311	ω(CH_2), δ(C5H9)
1329 w	1326 w	1329	1374	1361; 1375	ν(C1C7), β(C7N9H20), δ(CH)
1406 s h m	1390 s h w	1392	1388; 1392	1393	ν(C11C12), ω(CH_2), ν_{sym}(O13C12O14)
1423 m	1421 m				
1446 w	1442 w	1432	1429	1431	β(NH_2), δ(CH)
1463 m	1461 m	1438	1441; 1442	1436; 1438	ν(C1C2), ν(C5C6), δ(CH), β(CH_2)
1482 w	1483 m	1467	1464	1467	ν(C1C6), ν(C3C4), δ(CH), β(CH_2)
1560 m	1567 s h w	1557	1532; 1536	1553 (R); 1554 (IR)	β(NH_2), ν(C1C2), ν(C3C4), δ(CH), ν(C7=O8), ν_{as}(O13C12O14)
1591 vs	1600 vs	1584	1591; 1594	1590 (R); 1596 (IR)	β(NH_2), ν(C2C3), ν(C5C6), δ(CH)
1600 s m		1563	1565	1567 (R); 1572 (IR)	β(NH_2), ν(C1C6), ν(C3C4), δ(CH)
1631 s vw	1625 vs	1541	1594	1541 (R); 1549 (IR)	β(NH_2), ν_{as}(O13C12O14), ω(CH_2)
1653 s vw	1654 s		1617	1642	β(NH_2), ν(C7=O8), ν(C1C2), ν(C4C5), δ(CH)
1684 w	1685 s w	1650	1653	1563	β(NH_2), ν(C7=O8), ν(C1C2), ν(C4C5), δ(CH)
_	2917	2921	2936	2920	ν_{sym}(CH_2)
_	2946	2961	2982	2960	ν_{as}(CH_2)
_	2979	–	–	–	–

Table 4 (*continued*)

Experimental		Calculated			Assignments
Raman	IR	monomer	dimer I	dimer II	
_	3051	3060	3063	3058	$\nu_{as}(CH)$ out of phase
_	3079	3078	3080	3075	$\nu_{sym}(CH_2)$ out of phase
_		3095	3091	3095	$\nu_{as}(CH_2)$ in phase
_		3099	3099	3098	$\nu_{sym}(CH_2)$ out of phase
_	3199	–	–	–	–
_	3254	–	–	–	–
_	3301	–	–	–	–
_	3356	–	–	–	–
_	3386	–	–	–	–
_	3414	3416	3318	3251	$\nu_{sym}(NH_2)$
_	3590	3565	3444	3475	$\nu_{as}(NH_2)$

ν – stretching; β – bending; δ – in plane bending; ρ – rocking; τ – twisting; ω – wagging; as – asymmetric; *sym* – symmetricș; vw – very weak; w – weak; m – medium; s – strong; vs – very strong; IR – only IR active; R – only Raman active.

spectrum, this band is of very weak intensity. Rocking of AGM molecule is attributed to the 358 cm^{-1} band, with medium Raman and weak IR intensity. In both cases, the correspondent wavenumbers calculated on dimer II have the smallest difference relative to the experimental data. Both values are underestimated.

Another very strong band in the Raman spectrum is the one present at 269 cm^{-1}. We assigned a twisting of the benzene ring to this band – an out of plane deformation of the ring.

The medium Raman band observed at 154 cm^{-1} is broad. We assigned this band to a combination of CH_2 rocking and the same twisting of the benzene ring.

On a first glance, the overall shapes of the calculated IR and Raman spectra of AGM are not a facsimile of the experimental ones. Some of the FT-IR and Raman bands were very well reproduced by our calculations, such as 1591 cm^{-1} (Raman) and 1600 cm-1 (IR), 1329/1326 cm^{-1}, 1278/1279 cm^{-1}, 1095/1097 cm^{-1}, 935/934 cm^{-1}, 796/799 cm^{-1}, 763/765 cm^{-1}, etc (see Table 4). This made assigning their normal modes much easier. While for other bands, the differences in position/intensity are more notable, but not troubling, especially in the 1000–1700 cm^{-1} range, because of the approximations we took on choosing the models and level of theory. The models for which one wants to perform frequency calculations by using DFT methods are limited to the number of atoms. When a monomer is used, the vibrations corresponding to functional groups involved in intermolecular interactions (such as hydrogen bonds) will differ significantly because these interactions are not taken into account. This is the reason why we chose to different models of dimmers (Figs. 1 and 2). The four molecules of AGM from a unit cell are involved in three intermolecular hydrogen bonds – one between two of them, forming a dimer I, and the others, interacting with AGM molecules outside the unit cell, forming another dimer I, and a dimer II (Fig. 4a). As a result, the vibrational

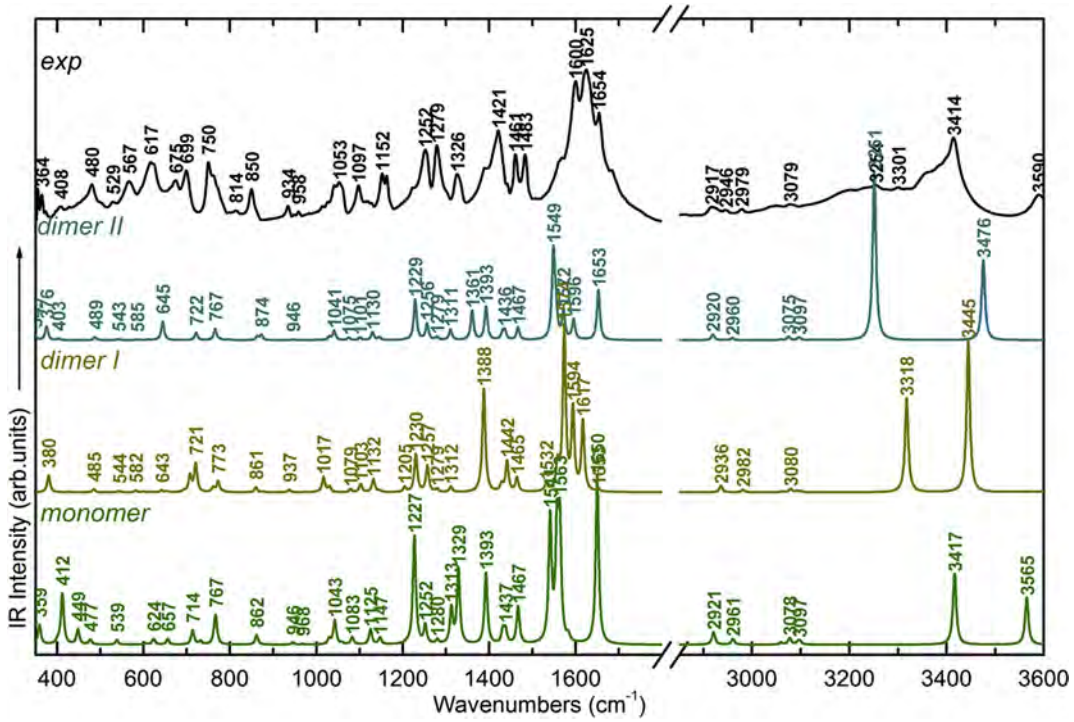

Fig. 11. Experimental FT-IR spectrum of AGM molecule in solid state, compared to calculated IR spectra on AGM monomer, dimer I, and dimer II. All calculations were performed at B3LYP/6-311 + G(2d,p) level of theory, in gas-phase.

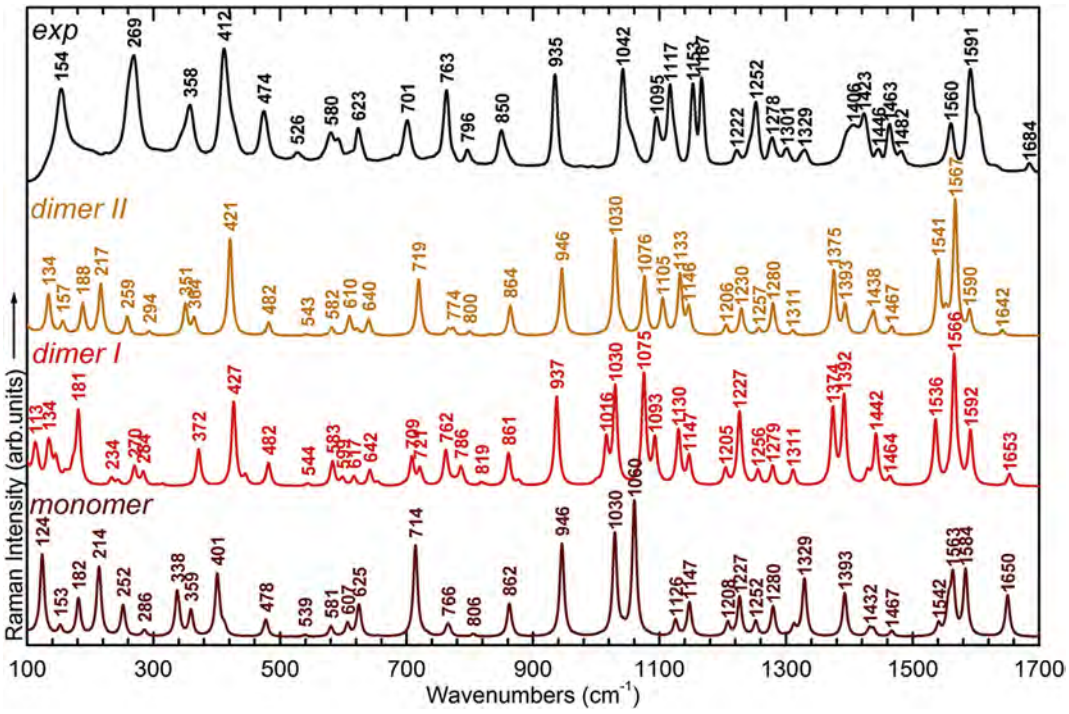

Fig. 12. Experimental Raman spectrum of AGM molecule in solid state (excitation laser line: 785 nm), compared to the calculated Raman spectra on AGM monomer, dimer I, and dimer II. All calculations were performed at B3LYP/6-311 + G(2d,p) level of theory, in gas-phase.

spectra should be a combination of the two dimmers'. Models consisting AGM molecules which present π-π stacking interactions (Fig. 4a) were not considered either. On the other hand, we did not take into account the anharmonicity when we performed the frequency calculations. This usually comes with discrepancies between our results and experimental data.

4.1. Influence of acidic media onto the sodium (2-carbamoylphenoxy) acetate salt

Being the salt of an active substance from the group of the salicylic acid derivatives, namely *o*-carbamoyl-phenoxyacetic acid, it is interesting to investigate the influence of slight amounts of hydrochloric acid onto the sodium salt structure.

Thus, the salt was treated with 0.2 M hydrochloric acid, considering a 1: 1.1 M ratio between salt and HCl. The X-ray diffraction pattern, FT-IR and Raman spectra of the final compound are presented in Fig. 13 (for comparison and a better understanding of the changes, the spectra of the initial structure are also presented).

From Fig. 13a, it can be observed that after treatment, a new structure was obtained and there are not at all traces of the starting material. The new compound was indexed by several indexing methods: TREOR90 [31], DICVOL96 [32] and X-Cell [33] using the Reflex module incorporated in the Biovia Materials Studio software [34]. Through all three indexing techniques, a monoclinic common solution ($a = 17.5567$ Å, $b = 4.8948$ Å, $c = 16.7413$ Å, $\beta = 114.68°$) with a relatively high figure of merit (F.O.M.) was obtained.

The vibrational data (both FT-IR and Raman) indicate the transformation of sodium salt in the corresponding acid: the appearing of new bands in the IR spectra, at 1713 and 3210 cm^{-1}, assigned to C═O and O—H stretching vibrations from the —COOH group, Fig. 13b, and the shift of the asymmetric stretching vibration of CO_2^- to higher frequency after the COOH formation (from 1684 to 1729 cm^{-1}), Fig. 13c [35].

5. Conclusions

The sodium (2-carbamoylphenoxy) acetate salt (denoted as AGM) crystallizes in triclinic system, and belongs to the P-1 space group, having four molecules in the asymmetric unit. The crystal structure of AGM shows that the compound comprises (2-carbamoylphenoxy) acetate (CBA) anions, sodium cations and one water molecule. Three cations of Na from the asymmetric unit are coordinated with six O atoms, while one Na cation with five oxygen atoms. The (2-carbamoylphenoxy) acetate anions and water molecules are held in the crystal structure also by N—H···O, O—H···O hydrogen bonds, four being intermolecular and nine intramolecular hydrogen bonds.

From the Hirshfeld analysis conducted on the four molecules of CBA and water, it appears that the strongest interactions which aggregate the structure are the coordination bonds between O^--Na^+ and the hydrogen bonds that contribute to the formation of the synthons. Fingerprint breakdown shows that the most numerous interactions are van der Waals (H···H, O···H/H···O, C···H/H···C) and coordinative (O···Na).

Two of (2-carbamoylphenoxy) acetate molecules from the asymmetric unit are coupled by inversion with neighbouring equivalent molecules, forming $R_2^2(8)$ and $R_2^2(18)$ supramolecular assemblies and the other two molecules of the asymmetric unit are coupled to each other by pseudo inversion forming a $R_2^2(18)$ synthon. If only the sodium cations are considered, they lay on both sides of the crystallographic plane (0 0 1), in the proximity of it.

FT-IR and Raman spectra of AGM are reported for the first time. We used calculated vibrational spectra on AGM monomer and two configurations of dimers for assigning the normal modes. In general, calculated modes on the two dimers are in better agreement with experimental data, especially for the normal modes belonging to the functional groups involved in hydrogen bonds. Dimer II provides better computational results above 1300 cm^{-1}, while dimer I performs a better fit for the modes below 1000 cm^{-1}. In

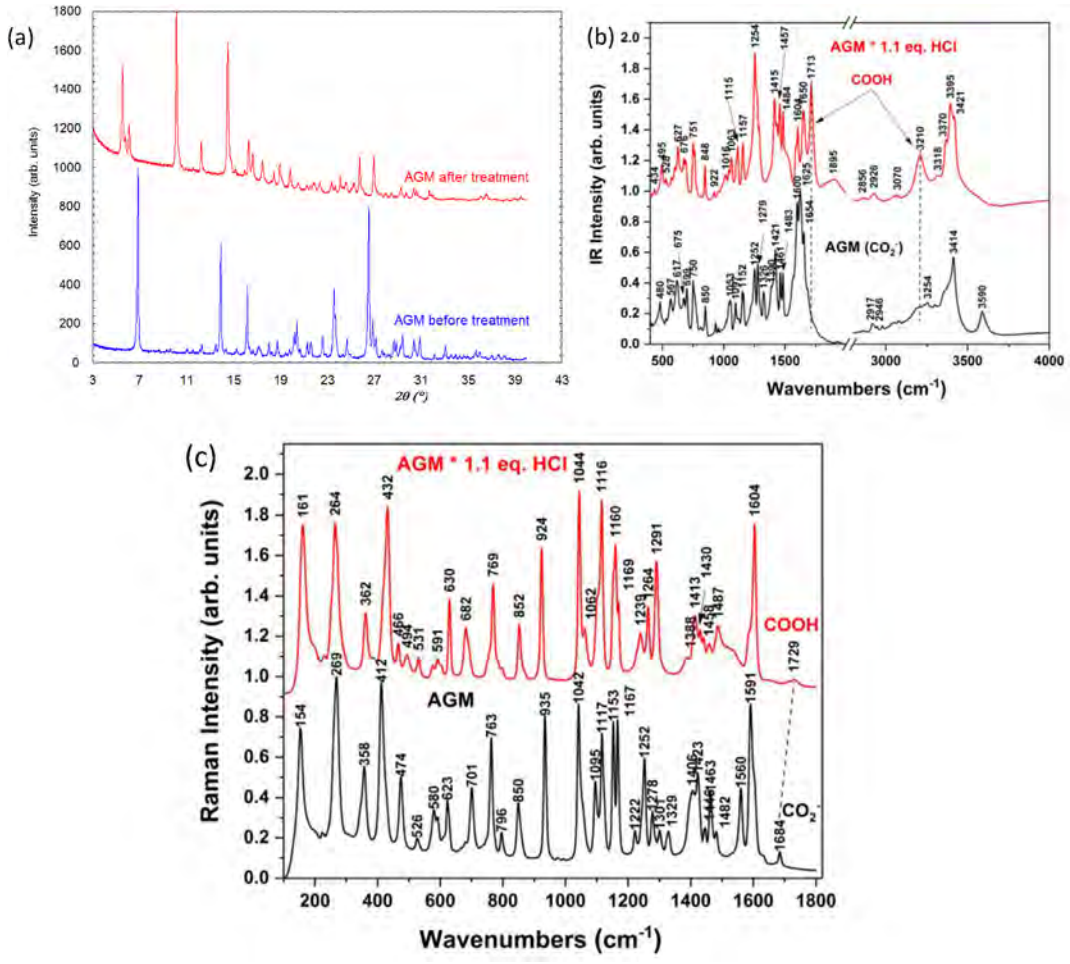

Fig. 13. X-ray diffraction (XRD) (a), FT-IR (b) and Raman (c) spectra of AGM before and after the treatment with 1.1 equivalents of 0.2 M hydrochloric acid.

between, both dimers present similar results. This emphasizes the importance of choosing a starting geometry that mimics as much as possible the real molecular interactions when calculating vibrational properties of molecules.

Declarations of interest

None.

Acknowledgments

This work was supported by a grant of Romanian Ministry of Research and Innovation, under Core Program, project number 19 35 02 02 (ATT, CBG) and 19 35 02 01 (AMRG, GB).

V. Chiș highly acknowledges the support of the CNCS-UEFISCDI Romania, grant PN–III–P4_ID-PCCF-2016-0112.

All calculations were performed on the high performance cluster supported by project POS CEE COD SMIS CSNR 48806/1862.

The authors would like to thank Sorina CIUPE for AGM's FT-IT spectrum.

Appendix A. Supplementary data

Supplementary data to this article can be found online at https://doi.org/10.1016/j.molstruc.2019.127016.

References

[1] MICROSIN products webpage. http://microsin.ro/products.php. (Accessed 2 August 2019).
[2] B. Meurer-Witt, J. Biehl, Rapidly Acting Analgesic for Treating Acute, Severe Pain, Comprises Intravenously Administered Aqueous Solution of O-Carbamoyl-Phenoxyacetic Acid, DE Patent DE10032224A1 2000.
[3] D. Loew, O. Schuster, G. Menke, J. Biehl, Pharmacokinetics of the analgesic o-carbamoylphenoxyacetic acid, Int. J. Clin. Pharmacol. Ther. Toxicol. 29 (1991) 124–129. https://www.ncbi.nlm.nih.gov/pubmed/2071259.
[4] M.A. Spackman, J.J. McKinnon, Fingerprinting intermolecular interactions in molecular crystals, CrystEngComm 4 (2002) 378–392. https://doi.org/10.1039/B203191B.
[5] J.J. McKinnon, D. Jayatilaka, M.A. Spackman, Towards quantitative analysis of intermolecular interactions with Hirshfeld surfaces, Chem. Commun. 0 (2007) 3814–3816. https://doi.org/10.1039/B704980C.
[6] M.A. Spackman, J.J. McKinnon, D. Jayatilaka, Electrostatic potentials mapped on Hirshfeld surfaces provide direct insight into intermolecular interactions in crystals, CrystEngComm (10) (2008) 377–388. https://doi.org/10.1039/B715227B.
[7] M.A. Spackman, D. Jayatilaka, Hirshfeld surface analysis, CrystEngComm (11) (2009) 19–32. https://doi.org/10.1039/B818330A.
[8] McKinnon, M.A. Spackmann, A.S. Mitchell, Novel tools for visualizing and exploring intermolecular interactions in molecular crystals, Acta Crystallogr. B (60) (2004) 627–668. https://doi.org/10.1107/S0108768104020300.
[9] N.E. Mircescu, M. Oltean, V. Chiș, N. Leopold, FTIR, FT-Raman, SERS and DFT study on melamine, Vib. Spectrosc. (62) (2012) 165–171. https://doi.org/10.1016/j.vibspec.2012.04.008.
[10] R. Luchian, E. Vinţeler, C. Chiș, M. Vasilescu, N. Leopold, V. Chiș, Molecular structure of phenytoin: NMR, UV-Vis and Quantum Chemical calculations, Croat. Chem. Acta (4) (2015) 88 511–522. https://doi.org/10.5562/cca2767.
[11] O.V. Dolomanov, L.J. Bourhis, R.J. Gildea, J.A.K. Howard, H.J. Puschmann, OLEX2: a complete structure solution, refinement and analysis program, Appl. Crystallogr. (42) (2009) 339–341. https://doi.org/10.1107/

S0021889808042726.
[12] L.J. Bourhis, O.V. Dolomanov, R.J. Gildea, J.A.K. Howard, H. Puschmann, The anatomy of a comprehensive constrained, restrained refinement program for the modern computing environment – olex2 dissected, Acta Crystallogr. (A71) (2015) 59–75. https://doi.org/10.1107/S2053273314022207.
[13] G.M. Sheldrick, Crystal structure refinement with SHELXL, Acta Crystallogr. C. C71 (2015) 3–8. https://doi.org/10.1107/S2053229614024218.
[14] CrysAlis RED Version 1.171.35.11, Oxford Diffraction Ltd., 2011.
[15] M.A. Spackman, P.G. Byrom, A novel definition of a molecule in a crystal, Chem. Phys. Lett. 267 (1997) 215–220. https://doi.org/10.1016/S0009-2614(97)00100-0.
[16] J.J. McKinnon, A.S. Mitchell, M.A. Spackman, Hirshfeld surfaces: a new tool for visualising and exploring molecular crystals, Chem. Eur J. (4) (1998) 2136–2141. https://doi.org/10.1002/(SICI)1521-3765(19981102)4:11<2136::AID-CHEM2136>3.0.CO;2-G.
[17] S.K. Wolff, D.J. Grimwood, J.J. McKinnon, M.J. Turner, D. Jayatilaka, M.A. Spackman, University of Western Australia, 2012.
[18] A.L. Rohl, M. Moret, W. Kaminsky, K. Claborn, J.J. Mckinnon, B. Kahr, Hirshfeld surfaces identify inadequacies in computations of intermolecular interactions in crystals: pentamorphic 1,8-dihydroxyanthraquinone, Cryst. Growth Des. (8) (2008) 4517–4525. https://pubs.acs.org/doi/10.1021/cg8005212.
[19] A. Parkin, G. Barr, W. Dong, C.J. Gilmore, D. Jayatilaka, J.J. Mckinnon, M.A. Spackman, C.C. Wilson, Comparing entire crystal structures: structural genetic fingerprinting, CrystEngComm (9) (2007) 648–652. https://doi.org/10.1039/B704177B.
[20] M.J. Frisch, H.B. Trucks, H.B. Schlegel, G.E. Scuseria, M.A. Robb, J.R. Cheeseman, G. Scalmani, V. Barone, B. Mennucci, G.A. Petersson, H. Nakatsuji, M. Caricato, X. Li, H.P. Hratchian, A.F. Izmaylov, J. Bloino, G. Zheng, J.L. Sonnenberg, M. Hada, M. Ehara, K. Toyota, R. Fukuda, J. Hasegawa, M. Ishida, T. Nakajima, Y. Honda, O. Kitao, H. Nakai, T. Vreven, J.A. Montgomery, J.E. Peralta, F. Ogliaro, M. Bearpark, J.J. Heyd, E. Brothers, K.N. Kudin, V.N. Staroverov, T. Keith, R. Kobayashi, J. Normand, K. Raghavachari, A. Rendell, J.C. Burant, S.S. Iyengar, J. Tomasi, M. Cossi, N. Rega, J.M. Millam, M. Klene, J.E. Knox, J.B. Cross, V. Bakken, C. Adamo, J. Jaramillo, R. Gomperts, R.E. Stratmann, O. Yazyev, A.J. Austin, R. Cammi, C. Pomelli, J.W. Ochterski, R.L. Martin, K. Morokuma, V.G. Zakrzewski, G.A. Voth, P. Salvador, J.J. Dannenberg, S. Dapprich, A.D. Daniels, O. Farkas, J.B. Foresman, J.V. Ortiz, J. Cioslowski, D.J. Fox, Gaussian 09, Revision B.01, Gaussian, Inc., Wallingford, CT, 2010.
[21] A.D. Becke, Density-functional thermochemistry. III. The role of exact exchange, J. Chem. Phys. 98 (1993) 5648–5652. https://doi.org/10.1063/1.464913.
[22] C. Lee, W. Yang, R.G. Parr, Development of the Colle-Salvetti correlation-energy formula into a functional of the electron density, Phys. Rev. B Condens. Matter 37 (1988) 785–789. https://doi.org/10.1103/PhysRevB.37.785.
[23] S.H. Vosko, L. Wilk, M. Nusair, Accurate spin-dependent electron liquid correlation energies for local spin density calculations: a critical analysis, Can. J. Phys. (58) (1980) 1200–1211. https://doi.org/10.1139/p80-159.
[24] P.J. Stephens, F.J. Devlin, C.F. Chabalowski, M.J. Frisch, Ab initio calculation of vibrational absorption and circular dichroism spectra using density functional force fields, J. Phys. Chem. 98 (1994) 11623–11627. https://pubs.acs.org/doi/abs/10.1021/j100096a001.
[25] M.P. Andersson, P. Uvdal, New scale factors for harmonic vibrational frequencies using the B3LYP density functional method with the triple-ζ basis set 6-311+G(d, p), J. Phys. Chem. A 109 (2005) 2937–2941. https://pubs.acs.org/doi/10.1021/jp045733a.
[26] R. Dennington, T.A. Keith, J.M. Millam, Semichem Inc., Shawnee Mission, KS, 2016.
[27] C.F. Macrae, I.J. Bruno, J.A. Chisholm, P.R. Edgington, P. McCabe, E. Pidcock, L. Rodriguez-Monge, R. Taylor, J. van de Streek, P.A. Wood, Mercury CSD 2.0 - new features for the visualization and investigation of crystal structures, J. Appl. Crystallogr. (41) (2008) 466–470. https://doi.org/10.1107/S0021889807067908.
[28] M.M. Ilczyszyn, T. Lis, M. Wierzejewska, Sodium dl-phenylglycinate trihydrate: structural, vibrational and theoretical studies, J. Mol. Struct. 937 (2009) 2–9. https://doi.org/10.1016/j.molstruc.2009.07.039.
[29] J. Pei, B. Yu, Hai-bin Song, X. qi Yan, Y. Zhang, X. Geng, Y. Wang, J. Yan, B. Sun, Synthesis, structure and spectrum studies on $Na_4(LM)_2(H_2O)_{12}$ (H_2LM=lumazine), J. Mol. Struct. 779 (2005) 43–48. https://doi.org/10.1016/j.molstruc.2005.07.025.
[30] S. Sasic, S. Ekins, Pharmaceutical Applications of Raman Spectroscopy, Wiley-Interscience,John Wiley & Sons, Inc., Hoboken, New Jersey, 2008.
[31] P.-E. Werner, L. Eriksson, M. Westdahl, TREOR, a semi-exhaustive trial-and-error powder indexing program for all symmetries, J. Appl. Crystallogr. 18 (1985) 367–370. https://doi.org/10.1107/S0021889885010512.
[32] A. Boultif, D. Louer, Powder pattern indexing with the dichotomy method, J. Appl. Crystallogr. 37 (2004) 724–731. https://doi.org/10.1107/S0021889804014876.
[33] M.A. Neumann, X-Cell, A novel indexing algorithm for routine tasks and difficult cases, J. Appl. Crystallogr. 36 (2003) 356–365. https://doi.org/10.1107/S0021889802023348.
[34] Dassault Systèmes BIOVIA, [Materials Studio], [v8.0.0.843], Dassault Systèmes, San Diego, 2014.
[35] G. Socrates, Infrared and Raman Characteristic Group Frequencies, third ed., Wiley-Interscience,John Wiley & Sons, Inc., Chichester, 2001.